Available online at www.sciencedirect.com
SCIENCE DIRECT
Thin Solid Films 497 (2006) 341 – 346
thin solid films
www.elsevier.com/locate/tsf

Structural and transport properties of heteroepitaxial $BaNb_xTi_{1-x}O_3$ ($x=0.05$, 0.2) thin films

Haizhong Guo, Lifeng Liu, Huibin Lu, Shuo Ding, Zhenghao Chen *

Beijing National Laboratory for Condensed Matter Physics, Institute of Physics, Chinese Academy of Sciences, P.O. Box 603, Beijing 100080, China

Received 7 March 2005; received in revised form 18 October 2005; accepted 31 October 2005
Available online 5 December 2005

Abstract

Heteroepitaxial $BaNb_xTi_{1-x}O_3$ ($x=0.05$, 0.2) thin films prepared on (100) MgO substrates have been studied by Micro-Raman spectroscopy, X-ray diffraction and electrical measurements. It is found that the $BaNb_{0.05}Ti_{0.95}O_3$ thin film is at tetragonal phase while the $BaNb_{0.2}Ti_{0.8}O_3$ thin film is at cubic phase. The measurement of temperature dependence of electrical resistivity shows that the $BaNb_{0.05}Ti_{0.95}O_3$ thin film is a semiconductor from 570 to 170 K, but the $BaNb_{0.2}Ti_{0.8}O_3$ thin film exhibits transitional conduction behavior between 570 and 78 K. Because of the two-dimensional compressive strain imposed on the film by the substrate, the phase transition characteristics for bulk $BaTiO_3$ (i.e, cubic to tetragonal to orthorhombic to rhombohedral) are absent in the films over the temperature range of 78 to 550 K.

PACS: 77.84.Dy; 78.30.-j; 73.50.-h
Keywords: $BaNb_xTi_{1-x}O_3$ thin films; Raman scattering; Transport property

1. Introduction

Barium titanate ($BaTiO_3$ or BTO) is one of the most studied perovskite ferroelectrics because of its dielectric, ferroelectric, excellent electro-optic and nonlinear optical properties [1–3]. Donor-doped barium titanates increase various interesting properties and device feasibilities [4–8]. When donor dopant Nb is incorporated into insulating $BaTiO_3$ (Nb : BTO), it offers a number of interesting physical properties making it an attractive material for applications. For example, due to its positive temperature coefficient of resistivity, Nb : BTO is used as PTC thermistors [9,10]. Chang et al. reported the photorefractive properties of BTO which were gradually modified by the addition of Nb [11]. On the other hand, it is also well known that oxygen vacancy [12] or impurity doping (e.g., Nb or La) [13,14] changes the electrical conductivity of BTO around room temperature. Yan et al. have reported that BTO can be changed from an insulator to an n-type semiconductor and finally to a metallic conductor with increasing content of doping Nb [15]. However, in bulk single crystal, a Nb concentration of 1 at.% is the limit of solid solution because of their unstable formation [9,10]. For films, however, much more Nb can possibly be doped into a BTO crystal structure [14–16]. Despite intense research activity in this field, presently available information concerning the lattice dynamics of Nb-doped BTO thin films is rather rare.

It is known that experimentally obtained parameters depend on the spatial magnitude and time scale of the measured physical phenomena. Micro-Raman spectroscopy, on the other hand, can provide local information because of the shorter coherence length and time scale of the phonons. Useful information about impurities, internal stress, and crystal symmetry has been obtained in various thin and ultrathin films [7,17–22]. Moreover, the structural changes associated with the phase transition usually have a large effect on Raman spectrum [7,23–25]. If stress is present in the material, it is possible to provide an estimate of the stress, as the phonon frequencies are strongly influenced by the presence of stress [18,19].

In the present work, heteroepitaxial $BaNb_xTi_{1-x}O_3$ ($x=0.05$, 0.2) thin films were grown on (100) MgO substrates by laser molecular beam epitaxy (LMBE). Micro-Raman spectroscopy, X-ray diffraction (XRD) and electrical measurements were performed to study the structural and transport

* Corresponding author. Tel.: +86 10 82649478; fax: +86 10 82649451.
E-mail address: zhchen@aphy.iphy.ac.cn (Z. Chen).

0040-6090/$ - see front matter © 2005 Elsevier B.V. All rights reserved.
doi:10.1016/j.tsf.2005.10.076

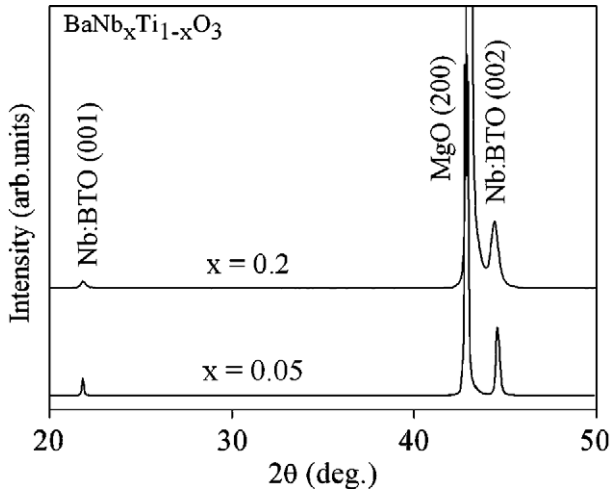

Fig. 1. X-ray $\theta-2\theta$ scan of the $BaNb_xTi_{1-x}O_3$ ($x=0.05$, 0.2) thin films on MgO substrates.

properties of the films. Experimental results suggest that the $BaNb_{0.05}Ti_{0.95}O_3$ thin film is at tetragonal phase, while the $BaNb_{0.2}Ti_{0.8}O_3$ thin film is at cubic phase at room temperature. The $BaNb_{0.05}Ti_{0.95}O_3$ thin film is a semiconductor from 570 to 170 K, while the $BaNb_{0.2}Ti_{0.8}O_3$ thin film exhibits transitional conduction behavior. Because of the two-dimensional compressive strain imposed on the film by the substrate, other phase transition characteristics for bulk $BaTiO_3$ are suppressed in the films.

2. Experimental details

Sintered bulk $BaNb_xTi_{1-x}O_3$ with $x=0.05$ and 0.2 was used as targets to fabricate the heteroepitaxial Nb:BTO thin films on MgO (100) substrates by LMBE. Monitored by In situ reflection high-energy electron diffraction, the Nb:BTO thin films were deposited layer by layer on single crystal MgO (100) substrates. Details of the growth conditions have been previously reported [16]. The substrate temperature, target-substrate distance, intensity and repetition frequency of the laser, and the oxygen pressure were all set to constant deposition conditions. The target-to-substrate distance was 4.5 cm. During the deposition, the substrates were heated up to 670 °C measured by an infrared thermometer. The epitaxy was carried out under the oxygen pressure of 3.0×10^{-4} Pa, and the thickness of thin films is 300 nm.

The crystallinity and phase purity of the Nb:BTO thin films were examined by XRD $\theta-2\theta$ scan and the asymmetric XRD {103} rocking curve measurement with Cu $K\alpha$ radiation [12,16]. The temperature dependence of the electrical resistance was measured between 77~570 K using van der Pauw method. Micro-Raman measurement for Nb:BTO thin films was performed in the backscattering geometry with a Jobin–Yvon T64000 triple Raman spectrometer. A 488 nm Ar^+ ion laser line was used for excitation. The sample was mounted on the cold finger end of a closed-cycle N_2 refrigerator. The spectrometer provided a wave number resolution of ~0.5 cm^{-1} and accuracy of ~0.1 cm^{-1}. The Raman spectra were measured in order of increasing temperature.

3. Results and discussion

Fig. 1 shows the $\theta-2\theta$ XRD scan curves of the Nb:BTO thin films. As can be seen from Fig. 1, there are no diffraction peaks from impurity phase or randomly oriented grains except MgO (l00) and Nb:BTO (00l) peaks, which means that the $BaNb_xTi_{1-x}O_3$ ($x=0.05$, 0.2) thin films are of single phase and orientation. The lattice parameters of a (in-plane lattice constant) and c (out-of-plane lattice constant), the calculated c/a ratios, and the unit cell volume $V^{1/3}$ getting from $(a^2c)^{1/3}$ as a function of the Nb doping content are summarized in Table 1. The lattice parameters c and a are obtained from (103) reflections [16]. Compared to the lattice parameters of the bulk BTO, the out-of-plane lattice constant of $BaNb_xTi_{1-x}O_3$ thin films are increased by 1.21% and 1.34% with $x=0.05$ and 0.2, respectively; the in-plane lattice constant of $BaNb_xTi_{1-x}O_3$ thin films are increased by 1.63% and 2.25% with $x=0.05$ and 0.2, respectively. This means that the films are stretched in the in-plane direction. In the meantime, the tetragonality of Nb:BTO films decreases with more Nb content in the films. The ratio c/a of the $BaNb_{0.05}Ti_{0.95}O_3$ thin film (1.0069) is more closer to that of bulk BTO (1.0110), and $BaNb_{0.05}Ti_{0.95}O_3$ thin film at tetragonal phase, while the ratio c/a of the $BaNb_{0.2}Ti_{0.8}O_3$ thin film (1.0019) is somewhat close to 1, and the $BaNb_{0.2}Ti_{0.8}O_3$ thin film is at near-cubic phase.

To investigate the transport properties, the temperature dependent resistivity (ρ) of the $BaNb_{0.05}Ti_{0.95}O_3$ and $BaNb_{0.2}Ti_{0.8}O_3$ thin films was measured by the van der Pauw method and has been plotted in Fig. 2(a) and (b), respectively. It can be seen from Fig. 2(a) that the $BaNb_{0.05}Ti_{0.95}O_3$ thin film exhibits an obvious semiconducting behavior from 570 to 170 K. It should be noted that the $BaNb_{0.2}Ti_{0.8}O_3$ thin film exhibits transitional conduction behavior between 570 and 78 K, and it is difficult to indicate the transition point but rather the transition interval (245–255 K), as shown in Fig. 2(b). This phenomenon may result from the diffusive transition behavior in thin films. The Hall measurement confirms that the charge carriers of the Nb:BTO thin films are n-type. The resistivity (ρ_{RT}), carrier concentration (n_H), and carrier mobility (μ_H) at room temperature are listed in Table 1. From Table 1 we can see that the value of the resistivity of the $BaNb_{0.2}Ti_{0.8}O_3$ thin

Table 1
Lattice parameters and electrical properties of $BaNb_xTi_{1-x}O_3$ ($x=0.05$, 0.2) thin films

x	a (Å)	c (Å)	c/a	$V^{1/3}$ (Å)	ρ_{RT} (Ω cm^{-1})	n_H (cm^{-3})	μ_H (cm^2 V^{-1} S^{-1})
0.05	0.4059	0.4087	1.0068	0.4068	5.68	3.03×10^{17}	3.3
0.2	0.4084	0.4092	1.0019	0.4086	1.08×10^{-2}	6.41×10^{19}	9.0
Bulk BTO	0.3994	0.4038	1.0110	0.4009	–	–	–

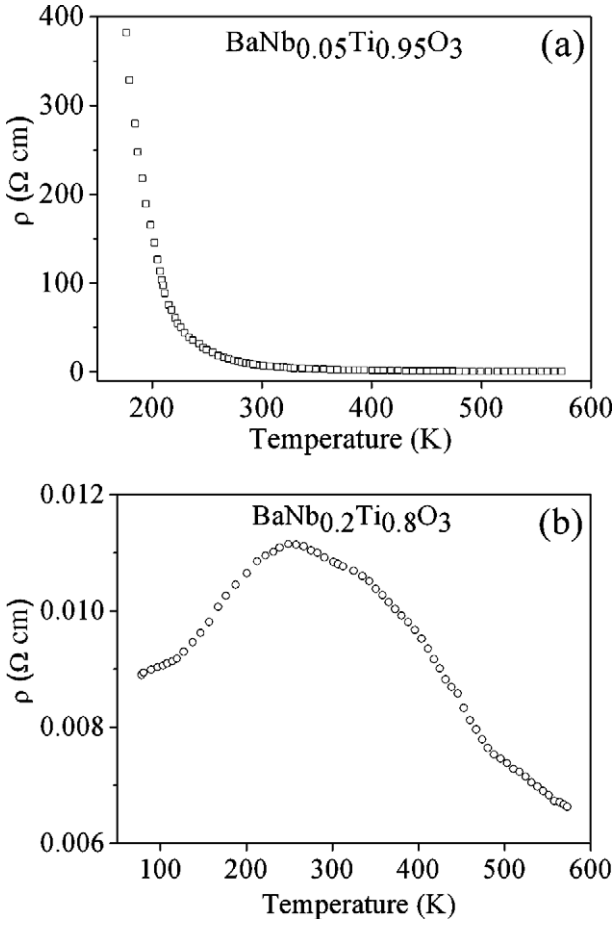

Fig. 2. The dependence of the electrical resistivity of the $BaNb_xTi_{1-x}O_3$ thin films with (a) $x=0.05$ and (b) $x=0.2$.

film is two orders of magnitude lower than that of the $BaNb_{0.05}Ti_{0.95}O_3$ thin film, while the value of the carrier concentration is two orders of magnitude larger than that of the $BaNb_{0.05}Ti_{0.95}O_3$ thin film. It is worthy to point out that the above data were approximately evaluated according to the conventional semiconductor coefficient measured at room temperature, although the problem of whether there is a simple relationship between Hall coefficient and carrier concentration is still under study.

Above 393 K, $BaTiO_3$ is cubic and belongs to space group $Fm3m$ (O_h^1). At temperature below 393 K, it is ferroelectric and its structure is $P4mm$ (C_{4v}^1), which further transforms into orthorhombic and rhombohedral structures at 278 and 183 K, respectively [26]. The cubic phase allows 12 optical modes ($3F_{1u}+1F_{2u}$) that are not Raman active. In the tetragonal phase, each triply degenerate F_{1u} mode splits into A_1+E modes, while the F_{2u} silent mode splits into B_1+E modes. Thus, $\Gamma_{tet}=3A_1+4E+B_1$. These modes further split into longitudinal (LO) and transverse (TO) components due to the long-range electrostatic forces associated with lattice ionicity. The assignment of phonons as LO or TO modes in the ferroelectric phase is valid as long as the phonon wave vector lies along one of the principal symmetry directions of the crystal. For the phonons propagating in between the principal axis, mixing of A_1 and E modes occurs and quasimodes are allowed in the spectra [26]. A detailed assignment of the vibrational frequencies on single crystalline BTO has been carried out using Raman spectroscopic results [27].

The room-temperature Raman spectra of Nb:BTO thin films and MgO substrate are shown in Fig. 3. It is noticeable that main typical features of BTO single crystal [27] have been clearly observed in the $BaNb_{0.05}Ti_{0.95}O_3$ thin film. The characteristic interference of the $A_1(TO_1)$ mode (~177 cm^{-1}) with a broad $A_1(TO_2)$ mode (~295 cm^{-1}) is due to the coupling between A_1 modes. Several investigators have studied this coupling phenomenon of A_1 modes in BTO [28,29]. A third asymmetric $A_1(TO_3)$ mode appears at about 527 cm^{-1} that also couples weakly with the $A_1(TO_2)$ mode. The $A_1(LO_1)$ mode associated with the tetragonal–cubic phase transition [27] is observed at 727 cm^{-1}. The appearance of $A_1(LO_1)$ mode (~727 cm^{-1}) clearly confirmed the tetragonal structure of the $BaNb_{0.05}Ti_{0.95}O_3$ thin film. Additionally, two new high frequency peaks at 827 and 870 cm^{-1} are present.

Raman spectra of the $BaNb_{0.2}Ti_{0.8}O_3$ thin film show some interesting changes. Firstly, the broad band at ~727 cm^{-1} becomes a plateau feature. Since the peak at ~727 cm^{-1} is a specific character for the tetragonal phase of BTO [27], the absence of the peak at ~727 cm^{-1} is an unambiguous indication of the absence of the tetragonal phase in the $BaNb_{0.2}Ti_{0.8}O_3$ thin film. This corresponds to the measurement of XRD, which indicates that the $BaNb_{0.2}Ti_{0.8}O_3$ thin film is at cubic phase. The plateau feature at approximately 700 cm^{-1} has also been observed in $BaZr_xTi_{1-x}O_3$ thin films at $x \geq 0.2$ [6,7]. Secondly, all the Raman peaks mentioned above are very broad and low in intensity. Thirdly, two broad bands at ~295 and 527 cm^{-1} persist in significant intensity in all the spectra. The existence of these broad bands in the cubic phase of single crystal and doped BTO has also been reported [30–32]. The origin of these broad bands seen in the cubic phase has been disputed for whether they are due to disorder-induced first-order or second-order Raman scattering. A recent temperature dependent Raman study on single crystal BTO clearly showed that these broad bands are first-order in character [31,32]. The

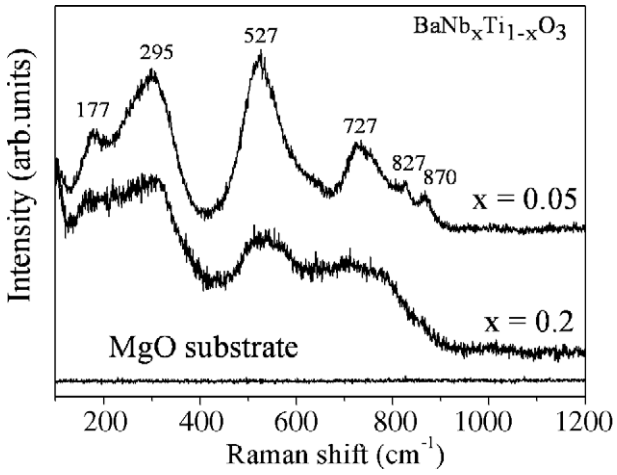

Fig. 3. Raman spectra of the $BaNb_xTi_{1-x}O_3$ thin films on MgO substrates with $x=0.05$ and $x=0.2$.

persistence of the first Raman bands in cubic phase was interpreted as due to the presence of disorder in the cubic phase [29]. Lastly, the Raman signal of two new high frequencies at 827 and 870 cm^{-1} vanishes.

The temperature dependence of the Raman spectra of the $BaNb_{0.05}Ti_{0.95}O_3$ and $BaNb_{0.2}Ti_{0.8}O_3$ thin films is presented in Fig. 4(a) and (b). Their temperature dependences are gradual and do not show sharp changes in the temperature range of 78–550 K. When temperature increases, the phonon lines broaden, but their frequencies are almost fixed. These behaviors indicate that the $BaNb_{0.05}Ti_{0.95}O_3$ and $BaNb_{0.2}Ti_{0.8}O_3$ thin films do not undergo any structural phase transition in the temperature range of 78–550 K. Although the measurements of the temperature dependence of electrical resistivity show that the $BaNb_{0.2}Ti_{0.8}O_3$ thin film exhibits transitional conduction behavior between 570 and 78 K, as shown in Fig. 2(b), the cubic to tetragonal, tetragonal to orthorhombic and orthorhombic to rhombohedral phase transitions for bulk $BaTiO_3$ are completely absent in the $BaNb_{0.2}Ti_{0.8}O_3$ and $BaNb_{0.05}Ti_{0.95}O_3$ thin films from 550 to 78 K.

The results of XRD and Raman scattering measurements clearly indicate that at room temperature the $BaNb_{0.05}Ti_{0.95}O_3$ thin film is crystallized into tetragonal structure, while the $BaNb_{0.2}Ti_{0.8}O_3$ thin film transforms into a disordered cubic structure. The reason of different structure for these two thin films can be elucidated as follows. There are two kinds of chemical bonds in $BaTiO_3$: the Ba–O bond and Ti–O bond. The Ti and O ions are not fully ionized because of the Ti ($3d$) and O ($2p$) hybridization. The tetragonal to cubic phase transition in BTO arises from a delicate cancellation between long-range electrostatic and short-range overlap forces [33]. The long-range electrostatic contribution to the energy greatly favors the tetragonal distortion. The short-range forces, however, greatly favor the undistorted cubic phase. The hybridization serves to reduce the overlap repulsion, softening the short-range forces so that the tetragonal distortion can take place. The substitution of Ti^{4+} (0.061 nm) by larger Nb^{5+} (0.064 nm) causes local distortions of the lattice structure, resulting in reduction of the long-range electrostatic with increase of the short-range forces, thus the cubic phase is stabilized with more Nb doping. On the other hand, it is known that, when Nb^{5+} donors are on the Ti^{4+} sites, a valence change of $Ti^{4+} \rightarrow Ti^{3+}$ can take place due to the compensation mechanism. A reduction of the Ti d hybridization due to the existence of d^1 in Ti^{3+} electron may be responsible for the stabilization of the cubic phase with more Nb doping.

As mentioned above, XRD studies show that there are no impurity phase or randomly oriented grains in the samples. High crystalline quality of the films allows to presume that a sport of structural defects of our film samples is unlikely to cause the suppressing of the phase transition characteristics existing in bulk $BaTiO_3$. Although we cannot completely exclude other factors, such as composition change or grain size effect, which can affect the properties, the strain in the thin films is the most probable cause for the phase transition behavior. Yuzyuk et al. [18,19] also observed using Raman measurements below room temperature that the low-temperature phase transition to rhombohedral phase in $Ba_{0.7}Sr_{0.3}TiO_3$/MgO thin film was completely suppressed. They suggested that the strong two-dimensional (2D) compressive stresses play an important role at the low-temperature phase transition. In our case, the compressive stresses in the Nb:BTO thin films might result from the lattice mismatch between the film and substrate, the thermal expansion coefficient difference between film and substrate, and the compositional change or deviation of the film [34,35]. These three factors are considered for Nb:BTO thin films as follows. First, due to lattice mismatch, the compressive strain of $u_m=(a_s-a_f)/a_f$, a_s is the effective lattice parameter of the substrate and a_f is the lattice constant of the free-standing film, and is fully relaxed at the growth temperature because the film thickness far exceeds the critical thickness which

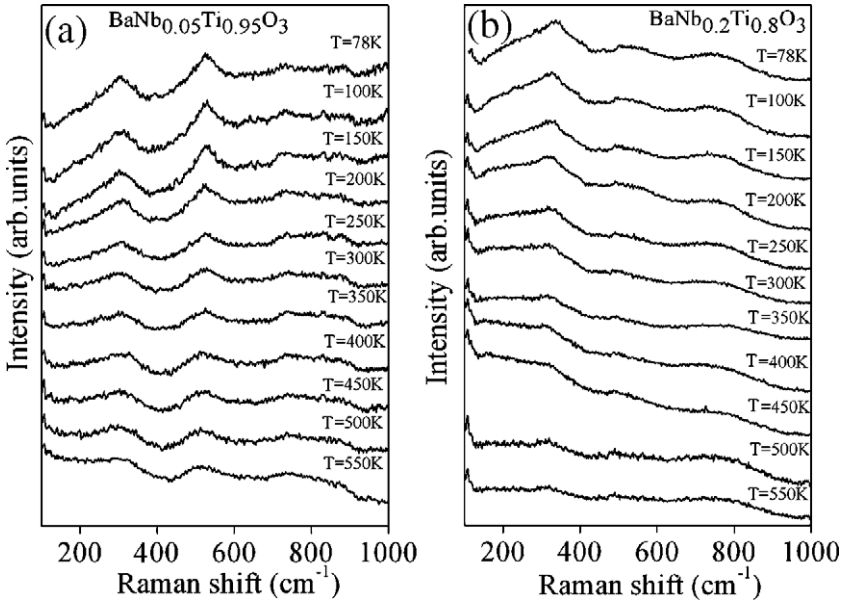

Fig. 4. Temperature dependence of the Raman spectra of the $BaNb_xTi_{1-x}O_3$ thin films on MgO substrates with (a) $x=0.05$ and (b) $x=0.2$.

is only few nanometers theoretically. So $u_m = 0$. Second, the strain due to the thermal expansion mismatch between the film and substrate is defined by the relation: $u_t = (\alpha_s - \alpha_f)(T - T_g)$, α_s and α_f are the linear thermal expansion coefficients of the substrate and the cubic phase of the films, respectively, and T_g, the growth temperature. The thermal expansion coefficients of MgO are larger than that of $BaTiO_3$ [36]. Consequently, when a $BaNb_xTi_{1-x}O_3$ film is cooled to room temperature after the deposition, it contracts less than that of the MgO substrate and a compressive strain is imposed on it. It is difficult to calculate the strain between 78–550 K because the thermal expansion coefficients of $BaNb_xTi_{1-x}O_3$ and MgO are temperature dependent. Finally, the compositional change due to the substitution of Ti^{4+} by larger Nb^{5+} causes the enlargement of the cell volume of the Nb:BTO thin films, inducing the decrease of the compressive strain of the sample with more Nb doping in the samples.

The strong 2D stresses in the samples result in an enhanced distortion of the films. These additional distortions give rise to Raman bands, which would be normally forbidden for the undistorted lattice. Since the compressive strain (proportional to ratio c/a) of the $BaNb_{0.05}Ti_{0.95}O_3$ thin film is larger than that of the $BaNb_{0.2}Ti_{0.8}O_3$ thin films, one can assume that the new Raman peaks at 828 and 870 cm^{-1} that were only observed in the $BaNb_{0.05}Ti_{0.95}O_3$ thin film may arise due to the static distortion. A large part of the Brillouin zone contributed to the scattering and the intensity of these modes is proportional to the Fourier transform of the static distortion. Thus, the observed broadening of the Raman lines in the samples reflects the influence of the strain field. It is known that 2D compressive stress results in an increase in the cubic–tetragonal transition temperature [37]. Accordingly, under the 2D compressive stress an upward shift of the transition temperature of the samples is expected. As it can be seen in Fig. 4, the $BaNb_{0.05}Ti_{0.95}O_3$ and $BaNb_{0.2}Ti_{0.8}O_3$ thin films do not undergo any phase transition in the temperature range 78–550 K. Moreover, due to the 2D compressive stress, the phase transition in thin films is usually diffused. Notice that the transport behavior of $BaNb_{0.2}Ti_{0.8}O_3$ thin film exhibits a broad transition interval between 245 and 255 K.

4. Conclusion

In summary, $BaNb_xTi_{1-x}O_3$ thin films were prepared with $x = 0.05$ and 0.2 on MgO substrates by LMBE. The results of XRD and Micro-Raman scattering demonstrated that the $BaNb_{0.05}Ti_{0.95}O_3$ thin film is at tetragonal phase while the $BaNb_{0.2}Ti_{0.8}O_3$ thin film at cubic phase. The measurements of temperature dependence of electrical resistivity show that the $BaNb_{0.05}Ti_{0.95}O_3$ thin film is a semiconductor from 570 to 170 K, while the $BaNb_{0.2}Ti_{0.8}O_3$ thin film exhibits transitional conduction behavior between 570 and 78 K. Raman spectra in the temperature range 78–550 K show that the phase transitions characteristic of bulk $BaTiO_3$ (cubic–tetragonal–orthorhombic–rhombohedral) are completely suppressed in the films. This behavior is explained by the presence of compressive stresses in the films.

Acknowledgments

The authors would like to thank Jianmin Hao for his help in XRD measurements and Yulong Liu for his help in Raman scattering measurements and many fruitful discussions. This work was supported by the key program for basic research of China.

Appendix A. Supplementary data

Supplementary data associated with this article can be found, in the online version, at doi:10.1016/j.tsf.2005.10.076.

References

[1] R.A. McKee, F.J. Walker, E.D. Specht, G.E. Jellison Jr., L.A. Boatner, Phys. Rev. Lett. 72 (1994) 2741.
[2] M. Sayer, K. Sreenivas, Science 247 (1990) 1056.
[3] R.E. Cohen, Nature (London) 358 (1992) 136.
[4] D. Rytz, B.A. Wecheler, M.H. Garrett, C.C. Nelson, R.N. Schwartz, J. Opt. Soc. Am. B 7 (1990) 2245.
[5] P.G. Schunemann, D.A. Temple, R.S. Hathcock, H.L. Tuller, H.P. Jessen, D.R. Gabbe, C. Warde, J. Opt. Soc. Am. B 5 (1988) 1685.
[6] R. Pantou, C. Dubourdieu, F. Weiss, J. Kreisel, G. Köbernik, W. Haessler, Mater. Sci. Semicond. Process. 5 (2002) 237.
[7] P.S. Dobal, A. Dixit, R.S. Katiyar, Z. Yu, R. Guo, A.S. Bhalla, J. Appl. Phys. 89 (2001) 8085.
[8] G. Yang, W.T. Wang, Y.L. Zhou, H.B. Lu, G.Z. Yang, Z.H. Chen, Appl. Phys. Lett. 81 (2002) 3969.
[9] S.H. Yoon, H. Kim, J. Appl. Phys. 92 (2002) 1039.
[10] S.S. Jida, T. Suemasu, T. Miki, J. Appl. Phys. 86 (1999) 2089.
[11] J.Y. Chang, C.F. Chu, C.Y. Huang, R.R. Yueh, J. Appl. Phys. 85 (1999) 2318.
[12] T. Zhao, Z.H. Chen, F. Chen, H.B. Lu, G.Z. Yang, Appl. Phys. Lett. 77 (2000) 4338.
[13] S.R. Gibert, L.A. Wills, B.W. Wessels, J.L. Schindler, J.A. Thomas, C.R. Kannewurf, J. Appl. Phys. 80 (1996) 969.
[14] D. Nagano, H. Funakubo, K. Shinozaki, N. Mizutani, Appl. Phys. Lett. 72 (1998) 2017.
[15] L. Yan, H.B. Lu, Z.H. Chen, S.Y. Dai, Y.L. Zhou, G.Z. Yang, J. Crystal Growth 225–228 (2002) 244.
[16] H.Z. Guo, L.F. Liu, S. Ding, H.B. Lu, Y.L. Zhou, B.L. Cheng, Z.H. Chen, J. Appl. Phys. 96 (2004) 3404.
[17] Yu.I. Yuzyuk, J.L. Sauvajol, P. Simon, V.L. Lorman, V.A. Alyoshin, I.N. Zakharchenko, E.V. Sviridov, J. Appl. Phys. 93 (2003) 9930.
[18] Yu.I. Yuzyuk, P. Simon, I.N. Zakharchenko, V.A. Alyoshin, E.V. Sviridov, Phys. Rev., B 66 (2002) 052103.
[19] Yu.I. Yuzyuk, R.S. Katiyar, V.A. Alyoshin, I.N. Zakarchenko, D.A. Markov, E.V. Sviridov, Phys. Rev., B 68 (2003) 104104.
[20] M.E.I. Marssi, F. Le. Marrec, I.A. Lukyanchuk, M.G. Karkut, J. Appl. Phys. 94 (2003) 3307.
[21] D.A. Tenne, A. Soukiassian, M.H. Zhu, A.M. Clark, X.X. Xi, H. Choosuwan, Q. He, R. Guo, A.S. Bhalla, Phys. Rev., B 67 (2003) 012302.
[22] A.A. Sirenko, I.A. Akimov, J.R. Fox, A.M. Clark, H.C. Li, W. Si, X.X. Xi, Phys. Rev. Lett. 82 (1999) 4500.
[23] T.Y. Kim, H.M. Jang, S.M. Cho, J. Appl. Phys. 91 (2002) 336.
[24] R. Naik, J.J. Nazarko, C.S. Flattery, U.D. Venkateswaran, V.M. Naik, M.S. Mohammed, G.W. Auner, Phys. Rev., B 61 (2000) 11367.
[25] G. Burns, B.A. Scott, Phys. Rev. Lett. 25 (1970) 167.
[26] J.D. Freire, R.S. Katiyar, Phys. Rev., B 37 (1988) 2074.
[27] C.H. Perry, D.B. Hall, Phys. Rev. Lett. 25 (1965) 700.
[28] A. Scalabrin, A.S. Chaves, D.S. Shim, S.P.S. Porto, Phys. Status Solidi, B 79 (1977) 731.
[29] J.A. Sanjarjo, R.S. Katiyar, S.P.S. Porto, Phys. Rev., B 22 (1980) 2396.
[30] A.M. Quittet, M. Lambert, Solid State Commun. 12 (1973) 1053.

[31] Y.J. Jiang, L.Z. Zeng, R.P. Wang, Y. Zhu, Y.L. Liu, J. Raman Spectrosc. 27 (1996) 31.
[32] L.M. Li, Y.J. Jiang, L.Z. Zeng, J. Raman Spectrosc. 27 (1996) 503.
[33] R.E. Cohen, H. Krakauer, Phys. Rev., B 42 (1990) 6416.
[34] D.A. Tenne, X.X. Xi, Y.L. Li, L.Q. Chen, A. Soukiassian, M.H. Zhu, A.R. James, J. Lettieri, D.G. Schlom, W. Tian, X.Q. Pan, Phys. Rev., B 69 (2004) 174101.
[35] M.S. Chen, Z.X. Shen, S.H. Tang, W.S. Shi, D.F. Cui, Z.H. Chen, J. Phys., Condens. Matter 12 (2000) 7013.
[36] V.G. Koukar, N.A. Pertsev, R. Waser, Phys. Rev., B 64 (2001) 214103.
[37] G.A. Rossetti Jr., L.E. Cross, K. Kushida, Appl. Phys. Lett. 59 (1991) 2524.